Noname manuscript No.
(will be inserted by the editor)

Fractional modeling of functionalized CNT suspensions

Jose Vicente Aguado[1], Emmanuelle Abisset-Chavanne[1], Elias Cueto[2], Francisco Chinesta[1], Roland Keunings[3]

Received: date / Accepted: date

Abstract Experimental findings and rheological modeling of chemically treated single-wall carbon nanotubes suspended in an epoxy resin were addressed in a recent publication Ma et al. (2009). The shear-thinning behaviour was successfully modeled by a Fokker-Planck based orientation model. However, the proposed model failed to describe linear viscoelasticity using a single mode as well as the relaxation after applying a finite step strain. Both experiments revealed a power-law behavior for the storage and relaxation moduli. In this paper, we show that a single-mode fractional diffusion model is able to predict these experimental observations.

Keywords Fractional derivatives · Functionalized CNTs · Small amplitude oscillatory flows · Linear Viscoelasticity

1 Introduction

The rheological modeling of untreated and chemically treated Carbon Nanotubes (CNTs) suspended in an epoxy resin was addressed in Ma et al. (2008) Ma et al. (2008). The resulting models were applied to simulate complex flows Cueto et al. (2008) Cueto et al. (2010).

The untreated CNT suspensions exhibited significant shear-thinning in steady state simple shear flow and contained optically resolvable aggregate structures depending on the applied shear rate Ma et al. (2008). A simple orientation model, based on a Fokker-Planck advection-diffusion description, failed to capture the experimentally observed rheological responses for untreated CNT suspensions. A new model named the 'Aggregation/
Orientation' (AO) model was then developed to describe the experimental findings Ma et al. (2008). A hierarchy of states between CNTs that are free from entanglement and a complete CNT network was incorporated into the AO model, thereby enabling different microstructure populations to exist for different shear conditions. Using a small number of adjustable parameters, it was found that the experimental data could be fitted with reasonable accuracy. A comparison between the rheology of CNTs and carbon black suspensions was carried out in Yearsley et al. (2012).

In the case of chemically treated CNTs suspended in an epoxy resin, the aggregation is prevented and we can consider that we are dealing with a large population of free rods in the dilute regime or rods experiencing interactions in the semi-concentrated or concentrated regimes. Thus, when a suspension of functionalized CNTs was subject to a steady shear flow, it exhibited shear-thinning behaviour, which was subsequently modelled by a Fokker-Planck (FP) based orientation model Ma et al. (2009). The model assumes that the shear flow aligns the CNTs in the flow direction, but there are events such as Brownian motion and tube-tube interactions that randomize the orientation. In the

[1]
GeM, UMR CNRS-Centrale Nantes
1 rue de la Noe, BP 92101, F-44321 Nantes cedex 3, France
E-mail: jose.aguado-lopez@ec-nantes.fr

[2]
I3A, Aragon Institute of Engineering Research
Universidad de Zaragoza, Maria de Luna s/n, Zaragoza, Spain

[3]
ICTEAM, Université catholique de Louvain
Bat. Euler, Av. Georges Lemaitre 4, B-1348 Louvain-la-Neuve, Belgium

FP orientation model, randomizing events were modelled with an appropriate rotary diffusion coefficient D_r and the shear-thinning behaviour was explained in terms of progressive alignment of CNTs towards the shear direction.

With regard to linear viscoelasticity (LVE), small-amplitude oscillatory measurements revealed mild elasticity for semi-dilute treated CNT suspensions. The exact origin for this elasticity is not clear and both tube-tube interactions and bending / stretching of CNTs have been proposed by other authors as possible origins (see Cruz et al. (2010) and the references therein).

Intuitively, chemical treatment creates a weakly interconnected network of CNTs and it is believed that the mild elasticity originates from this weak network as well as other randomizing events (Brownian motion and tube-tube hydrodynamic interactions). Step strain experiments confirmed the presence of a weak network at small strains, which was found to be destroyed at large strains.

Brownian dynamics modeling was addressed in Cruz et al. (2010) Cruz et al. (2012), where the elasticity effects were explained as a direct consequence of the bending of CNTs having a non-straight natural configuration due to side-wall defects.

Experimental LVE data of the treated CNT suspensions were fitted in Ma et al. (2009) using the FP orientation model with an effective diffusion coefficient term. An empirical relation was subsequently identified for the effective diffusion term that assumed a dependency of the diffusion coefficient on the applied frequency in order to avoid the introduction of a large number of relaxation mechanisms that are difficult to support on physical grounds.

It should be noticed, however, that such an approach based on the use of a single mode and a diffusion coefficient depending on the applied frequency is inconsistent. Indeed, we firstly assumed linearity, i.e. a diffusion coefficient independent on the applied frequency. Then, in order to fit the experimental results, the diffusion coefficient was assumed dependent on the applied frequency. Thus, from a linear assumption we concluded on a nonlinear behaviour that invalidated the analysis carried out. Concerning the relaxation after applying a finite step strain, the model presented in Ma et al. (2009) was unable to describe the experimental results that again exhibit a power-law evolution instead of the exponential one that the proposed model predicted.

In this paper, we revisit the experimental results reported in Ma et al. (2009) concerning chemically treated CNTs, in particular those related to LVE and step strain relaxation after applying a finite step strain. We show that a fractional diffusion model with a single mode only is able to predict the power-law behaviour observed in both experiments.

2 Experimental details

In what follows, we briefly summarize the experiments carried out by Ma and Mackley in Cambridge, whose results were reported in Ma et al. (2009).

Single-walled CNTs were produced by High Pressure carbon monoxide disproportionation that were supplied by Nanocomposites Inc., USA. In the case of treated CNTs, aggregation was prevented by covalently attaching arene diazonium salts onto the sidewall of CNTs. The treated CNT suspensions were stablilised via electrostatic repulsion between CNTs.

Microstructure of resulting mixtures was optically characterized using the Cambridge Shear System. Optical analysis proved that the suspension showed no optically resolvable aggregates of CNTs, and the mixture was well-dispersed at the micron-level. By contrast, the untreated CNT suspension consisted of optically resolvable CNT aggregates Rahatekar et al. (2006).

Rheological measurements were made using an ARES strain-controlled rheometer with $50mm$ parallel plates and a gap size of $0.3mm$. In the small-amplitude oscillatory shear experiment, a strain amplitude of 1% was used. In order to minimize possible complication from sample loading, samples were slowly squeezed between the parallel plates and were rested for at least two hours before any measurements were carried out. Step strain experiments were carried out in order to explore the transition from small to large strain deformations.

Linear viscoelasticity (LVE) of CNT suspensions was studied using small-amplitude oscillatory measurements. Epoxy resin showed scattered G' data with torque values very close to the detection limit of the transducer, implying that the elasticity of the matrix is negligible ($G'_{epoxy} \approx 0$). Epoxy behaved essentially as a Newtonian fluid with viscous dissipation that is consistent with steady shear measurements. Addition of CNTs increased the values of both G' and G'' as reported in Ma et al. (2009). Measurements were made at a strain of 1%, which was well within the linear strain response of the suspensions. The enhancement of G' was concentration dependent and was more pronounced at high concentration levels (0.2% and 0.5%). The evolution of G' as a function of frequency is consistent with experimental results reported by others Song ang Young (2005) Xu et al. (2005). Addition of CNTs increased the elasticity of the system as a whole Ma et al. (2009). This response is very different from that of a typical short fibre suspension, where addition of fibres was reported

to have no extra contribution to the storage modulus G' of the suspending medium Carter (1967) Ganani and Powell (1986).

To assess the relative importance of viscous and elastic contributions at a given concentration, we show in Fig. 1 the obtained data for G', G'' and η^* for the 0.5% CNT suspension. The value of G'' was observed to be higher than G' within the full range of frequency studied, which implies that elasticity associated with the addition of CNTs is mild. Although the elastic response is relatively weak, it is interesting to note that the experimental evolution of G' and G'' does not follow the prediction of a single-mode Maxwell model.

A series of step strain experiments were carried out in order to reveal more detailed relaxation behaviour of the treated CNT suspensions and to offer insights into the origin of elasticity. A finite step strain (γ_0) was applied to the CNT suspensions and the process of stress relaxation was followed using the strain-controlled ARES rheometer. Figure 2 shows the time evolution of the relaxation modulus (G), which is defined as $G = \frac{\tau}{\gamma_0}$, for a 0.5% CNT suspension for different values of the step strain. The stepper motor had a response time of about 0.1s (as indicated in the figure) and for the epoxy matrix, the stress dissipated almost instantaneously, consistent with the fact that it behaved essentially as a simple Newtonian fluid in both steady shear and LVE experiments. Addition of CNTs prolonged the stress relaxation process, with the CNT suspensions showing a viscoelastic response. The effect was progressive as the CNT concentration increased and this confirmed the earlier LVE experiments that addition of CNTs effectively increases the elasticity of the system as a whole.

Strains of different magnitude were applied to the 0.5% CNT suspension. Figure 2 shows a strain dependence in terms of the final mode of stress relaxation. At small strains (1%, 5% and 10%), the CNT suspension responded essentially as an entangled gel. At high strain, the CNT suspension behaved in a dominantly viscous fluid manner. Intuitively, the strain-dependence relaxation process can be explained by the yielding of a network Amari and Watanabe (1980) Mewis and Meire (1984). Depending on the strength of the network, if a large enough strain is applied, the network will be broken down and will finally dissipate as a fluid. The network for the 0.5% suspension is considered to be a relatively weak one and it broke down at a strain level higher than 10%. These findings have two implications. Firstly, it is highly probable that the mild elasticity observed in LVE measurements is linked to the presence of a weak CNT network. Secondly, the effect of elasticity is negligible at high strain level, in line with the nonlinear experiments reported in Ma et al. (2009) that

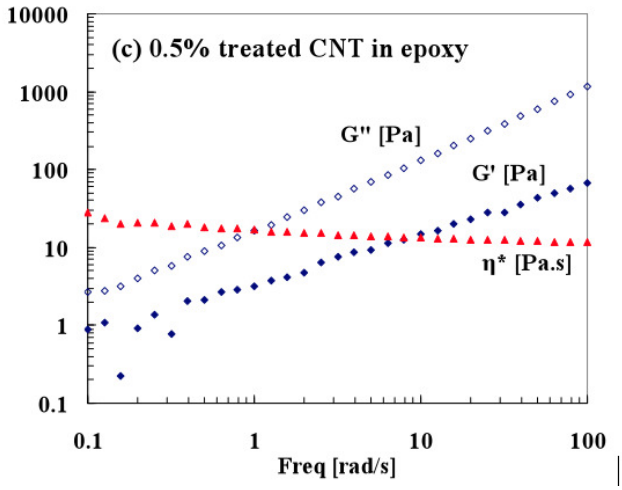

Fig. 1 Linear viscoelastic (LVE) data, which include the storage modulus G', the loss modulus G'' and the complex viscosity η^* as a function of frequency, for the 0.5% treated CNT suspension (source Ma et al. (2009))

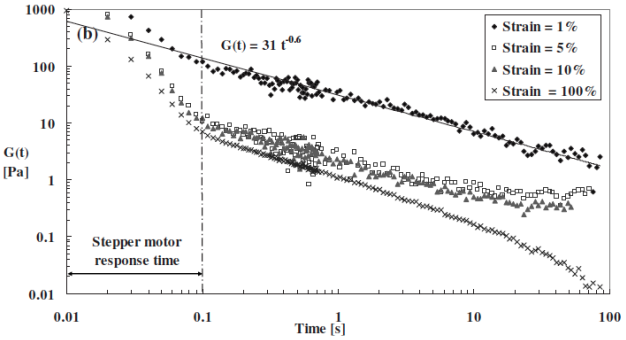

Fig. 2 Stress relaxation data for the 0.5% CNT suspension with varying magnitudes of step strain (source Ma et al. (2009))

revealed small diffusion effects attributed to Brownian effects and tube-tube hydrodynamic interactions.

3 Standard modeling

A standard modeling study was carried out in Ma et al. (2009) by considering Brownian suspensions involving rods (ellipsoids of infinite aspect ratio). The main ingredients of the model are summarized in this section. For a more detailed discussion of the multiscale modeling of non-Brownian and Brownian suspensions of rods, see Chinesta (2013).

The extra-stress tensor of the suspension is given by

$$\boldsymbol{\tau} = 2\eta\mathbf{D} + 2\eta N_p\left(\mathbf{D}:\mathbf{A}\right) + \beta D_r\left(\mathbf{a} - \frac{\mathbf{I}}{d}\right), \qquad (1)$$

where η is the viscosity of the suspending fluid (epoxy resin), $\mathbf{D}$ is the rate of strain tensor (symmetric part

of the velocity gradient tensor $\nabla\mathbf{v}$), N_p is the particle number that depends on the rod concentration, and $\mathbf{a}$ and $\mathbf{A}$ are the second and fourth-order orientation tensors respectively defined as Advani and Tucker (1987) Advani and Tucker (1980)

$$\mathbf{a}(\mathbf{x},t) = \int_{\mathcal{S}} \mathbf{p}\otimes\mathbf{p}\ \psi(\mathbf{x},t,\mathbf{p})\ d\mathbf{p}, \tag{2}$$

and

$$\mathbf{A}(\mathbf{x},t) = \int_{\mathcal{S}} \mathbf{p}\otimes\mathbf{p}\otimes\mathbf{p}\otimes\mathbf{p}\ \psi(\mathbf{x},t,\mathbf{p})\ d\mathbf{p}, \tag{3}$$

where the unit vector $\mathbf{p}$ defines the rod orientation, $\mathcal{S}$ is the surface of the unit ball, and $\psi(\mathbf{x},t,\mathbf{p})$ is the orientation distribution function that gives the fraction of rods that at position $\mathbf{x}$ and time t are aligned along the direction $\mathbf{p}$; D_r is a diffusion coefficient, β is a parameter affecting the diffusion term, $\mathbf{I}$ is the unit tensor and d is the dimension of physical space ($d = 2$ or 3).

The evolution equation for the second-order orientation tensor was derived in detail in Chinesta (2013):

$$\dot{\mathbf{a}} = \nabla\mathbf{v}\cdot\mathbf{a} + \mathbf{a}\cdot(\nabla\mathbf{v})^T - 2\mathbf{A}:\mathbf{D} - 2dD_r\left(\mathbf{a} - \frac{\mathbf{I}}{d}\right). \tag{4}$$

In order to close the model, a suitable closure relation expressing $\mathbf{A}$ as a function of $\mathbf{a}$ is needed. Among the numerous available closure relations, we consider in what follows the linear closure relation that becomes exact for an isotropic distribution function Advani and Tucker (1980).

3.1 LVE modeling

As LVE involves a small amplitude oscillation applied to an essentially isotropic suspension ($\mathbf{a}^{iso} \approx \frac{\mathbf{I}}{3}$), the linear closure relation is expected to be an accurate approximation for describing $\mathbf{A}$. The linear closure reads Advani and Tucker (1980):

$$\mathbf{A}^{lin}_{ijkl}(\mathbf{a}) = -\frac{1}{35}\left(\mathbf{I}_{ij}\mathbf{I}_{kl} + \mathbf{I}_{ik}\mathbf{I}_{jl} + \mathbf{I}_{il}\mathbf{I}_{jk}\right) +$$

$$\frac{1}{7}\left(\mathbf{a}_{ij}\mathbf{I}_{kl} + \mathbf{a}_{ik}\mathbf{I}_{jl} + \mathbf{a}_{il}\mathbf{I}_{jk} + \mathbf{a}_{kl}\mathbf{I}_{ij} + \mathbf{a}_{jl}\mathbf{I}_{ik} + \mathbf{a}_{jk}\mathbf{I}_{il}\right). \tag{5}$$

To predict the shear stress $\boldsymbol{\tau}_{12}$, we need to compute the component $(\mathbf{A}:\mathbf{a})_{12}$ as well as the component $\mathbf{a}_{12}$ involved in the diffusion term of Eq. (1). Taking into account that the applied flow (small amplitude oscillation) implies the strain rate

$$\mathbf{D} = \begin{pmatrix} 0 & \frac{\dot\gamma}{2} & 0 \\ \frac{\dot\gamma}{2} & 0 & 0 \\ 0 & 0 & 0 \end{pmatrix}, \tag{6}$$

and that it only induces a small perturbation of the isotropic orientation state $\mathbf{a}^{iso}$,

$$\mathbf{a}^{iso} = \begin{pmatrix} \frac{1}{3} & 0 & 0 \\ 0 & \frac{1}{3} & 0 \\ 0 & 0 & \frac{1}{3} \end{pmatrix}, \tag{7}$$

the linear closure approximation (5) yields $(\mathbf{A}:\mathbf{D})_{12} \approx (\mathbf{A}^{lin}(\mathbf{a}^{iso}):\mathbf{D})_{12} = \frac{\dot\gamma}{15}$.

Thus, the shear stress can be approximated in the general 3D case by

$$\boldsymbol{\tau}_{12} \approx \eta\dot\gamma + \frac{2}{15}\eta N_p\dot\gamma + \beta D_r\mathbf{a}_{12}, \tag{8}$$

wherein we can identify a viscous component (the one affected by $\dot\gamma$) and an elastic one (the one that does not depend on $\dot\gamma$). Obviously, elastic effects will be associated to the last contribution that in fact corresponds to diffusion effects that depend linearly on the component $\mathbf{a}_{12}$. In order to evaluate the time evolution of $\mathbf{a}_{12}$, we consider Eq. (4) in the general 3D case ($d = 3$):

$$\dot{\mathbf{a}} = \nabla\mathbf{v}\cdot\mathbf{a} + \mathbf{a}\cdot(\nabla\mathbf{v})^T - 2\cdot\mathbf{A}:\mathbf{D} - 6D_r\left(\mathbf{a} - \frac{\mathbf{I}}{3}\right). \tag{9}$$

Now, using the same approximations as in the previous paragraphs, we obtain $(\nabla\mathbf{v}\cdot\mathbf{a} + \mathbf{a}\cdot(\nabla\mathbf{v})^T - 2\cdot\mathbf{A}:\mathbf{D})_{12} \approx \frac{\dot\gamma}{5}$. Thus, Eq. (9) reduces to

$$\dot{\mathbf{a}}_{12} \approx \frac{\dot\gamma}{5} - 6D_r\mathbf{a}_{12}. \tag{10}$$

For the sake of notational simplicity, we define $\mathbf{a}_{12} \equiv a$ and $\boldsymbol{\tau}_{12} \equiv \tau$. Thus, the LVE model reads:

$$\begin{cases} \tau \approx \eta\dot\gamma + \frac{2}{15}\eta N_p\dot\gamma + \beta D_r a \\ \dot a \approx \frac{\dot\gamma}{5} - 6D_r a \end{cases}. \tag{11}$$

Now, let us apply the small amplitude oscillation $\gamma(t)$ given by

$$\gamma = \gamma_0 e^{i\omega t}, \tag{12}$$

with $i = \sqrt{-1}$, that results in the shear rate

$$\dot\gamma = i\omega\gamma_0 e^{i\omega t}. \tag{13}$$

From the second equation in (11), we can expect that $a(t)$ has the same oscillation frequency but with a certain phase delay φ, that is

$$a = a_0 e^{i\omega t - i\varphi} = \tilde a_0 e^{i\omega t}. \tag{14}$$

Introducing expressions (13) and (14) into the second equation in (11) and using the notations considered in Ma et al. (2009) $\lambda = \frac{1}{6D_r}$ and $\mu = \frac{1}{30D_r}$, we obtain

$$i\omega\lambda\tilde a_0 + \tilde a_0 = i\omega\mu\gamma_0, \tag{15}$$

from which we have

$$\tilde{a}_0 = \left(\frac{\lambda\mu\omega^2}{1+\lambda^2\omega^2} + i\frac{\mu\omega}{1+\lambda^2\omega^2} \right) \gamma_0. \tag{16}$$

With this result, we go back to the stress expression (first equation in (11)) and write the complex stress amplitude according to:

$$\begin{aligned} \tilde{\tau} =& \gamma_0 \left(i\omega\eta \left(1 + \frac{2}{15} N_p \right) + \right. \\ & \left. \beta D_r \left(\frac{\lambda\mu\omega^2}{1+\lambda^2\omega^2} + i\frac{\mu\omega}{1+\lambda^2\omega^2} \right) \right), \end{aligned} \tag{17}$$

from which we can identify the storage and loss moduli,

$$\begin{cases} G' = \frac{\Re(\tilde{\tau})}{\gamma_0} \\ G'' = \frac{\Im(\tilde{\tau})}{\gamma_0} \end{cases}, \tag{18}$$

where $\Re(\tilde{\tau})$ and $\Im(\tilde{\tau})$ denote the real and imaginary part of $\tilde{\tau}$ respectively. We obtain

$$G' = \beta D_r \frac{\lambda\mu\omega^2}{1+\lambda^2\omega^2}, \tag{19}$$

and

$$G'' = \omega\eta \left(1 + \frac{2}{15} N_p \right) + \beta D_r \frac{\mu\omega}{1+\lambda^2\omega^2}. \tag{20}$$

Thus, the loss modulus scales linearly with the frequency ω of the applied oscillation in agreement with the experimental findings.

The storage modulus G' scales at small frequencies with the square ω^2 of the applied frequency. This result, however, is inconsistent with the experimental findings reported in Ma et al. (2009). See Fig. 1, wherein the storage modulus is observed to scale roughly as $\omega^{0.6}$.

In Eq. (19), we notice that D_r appears at the power -1 as both μ and λ are proportional to D_r^{-1}. Thus, by assuming D_r proportional to an adequate power p of the applied frequency ω, i.e. $D_r \propto \omega^p$, one could control the fitting process. This was the route considered in Ma et al. (2009). It is important, however, to emphasize that this route implies a certain inconsistency: assuming a frequency-dependent diffusion coefficient implies a non-linear behaviour, while the entire analysis is based on a linearity assumption. The authors followed this route in Ma et al. (2009) to avoid the introduction of many relaxation modes.

These relaxation modes could be associated with the poly-dispersity, with thermally activated bending, flow induced bending in the case of non-straight CNTs as proposed in Cruz et al. (2010) Cruz et al. (2012). However, in absence of the required information the use of multiple modes reduces to the simple identification of the associated parameters.

In section 4, we propose an alternative, consistent and physically supported approach based on the concept of fractional derivatives.

3.2 Step strain modeling

After applying the step strain, the stress relaxation results from Eq. (1), assuming the fluid at rest:

$$\tau = \beta D_r a, \tag{21}$$

where again $\tau = \boldsymbol{\tau}_{12}$ and $a = \mathbf{a}_{12}$. The evolution of a can be calculated from Eq. (4), that in absence of flow reduces to

$$\frac{da}{dt} = -6D_r a. \tag{22}$$

This yields an exponential decay for a and, consequently, the same decay for the shear stress τ. As discussed in Ma et al. (2009), the predicted exponential decay does not agree with the power-law behaviour observed experimentally.

4 Fractional modeling

In complex fluids, micro-rheological experiments often exhibit anomalous sub-diffusion or sticky diffusion, in which the mean square displacement of Brownian tracer particles is found to scale as $\langle x^2 \rangle \propto t^\alpha$ with $0 < \alpha < 1$ (see Jaishankar and McKinley (2012) and the references therein). In these cases, the use of non-integer derivatives can constitute an appealing alternative as it allows one to correctly reproduce the observed physical behaviour while keeping the model as simple as possible. Moreover, from a physical point of view, the use of non-integer derivatives introduces a degree of non-locality that seems in agreement with the intrinsic nature of the physical system.

In the case of semi-dilute and semi-concentrated suspensions of functionalized CNTs, chemical treatment creates a weakly interconnected network of CNTs responsible of the mild elasticity experimentally observed. In a such a percolated system Brownian motion is expected to be disturbed exhibiting the just referred anomalous diffusion.

It is well known that standard diffusion mechanisms imply a Brownian velocity $\dot{\mathbf{p}}|^B$

$$\dot{\mathbf{p}}|^B = -D_r \frac{\frac{\partial\psi}{\partial\mathbf{p}}}{\psi}, \tag{23}$$

that leads to the equations considered in the previous section.

A fractional counterpart consists in generalizing Eq. (23) by assuming a non-integer time derivative:

$$\left. \frac{d^\alpha \mathbf{p}}{dt^\alpha} \right|^B = -D_r \frac{\frac{\partial\psi}{\partial\mathbf{p}}}{\psi}, \tag{24}$$

where one could expect from the experimental data that $\alpha < 1$. See Appendix A for additional information on fractional derivatives.

Now, in view Eq. (2), the time derivative of the second-order orientation tensor $\mathbf{a}$ reads

$$\frac{d\mathbf{a}}{dt} = \int_{\mathcal{S}} \left(\dot{\mathbf{p}} \otimes \mathbf{p} + \mathbf{p} \otimes \dot{\mathbf{p}}\right)\ \psi\ d\mathbf{p}. \tag{25}$$

Here, the effective rotary velocity $\dot{\mathbf{p}}$ is given by

$$\dot{\mathbf{p}} = \dot{\mathbf{p}}|^J + \dot{\mathbf{p}}|^B, \tag{26}$$

where $\dot{\mathbf{p}}|^J$ is the flow-induced velocity expressed from Jeffery's equation Chinesta (2013)

$$\dot{\mathbf{p}}|^J = \nabla\mathbf{v} \cdot \mathbf{p} - \left(\nabla\mathbf{v} : (\mathbf{p} \otimes \mathbf{p})\right)\mathbf{p}, \tag{27}$$

and $\dot{\mathbf{p}}|^B$ is the velocity related to fractional diffusion,

$$\dot{\mathbf{p}}|^B = -D_r \frac{d^{1-\alpha}}{dt^{1-\alpha}} \left(\frac{d^\alpha \mathbf{p}}{dt^\alpha}\bigg|^B\right) = -D_r \frac{d^{1-\alpha}}{dt^{1-\alpha}} \left(\frac{\frac{\partial \psi}{\partial \mathbf{p}}}{\psi}\right). \tag{28}$$

Introducing the effective rotary velocity into Eq. (25) and proceeding as described in Appendix B, we obtain

$$\frac{d\mathbf{a}}{dt} = \dot{\mathbf{a}}|^J - 2dD_r \frac{d^{1-\alpha}}{dt^{1-\alpha}} \left(\mathbf{a} - \frac{\mathbf{I}}{d}\right), \tag{29}$$

with $\dot{\mathbf{a}}|^J = \nabla\mathbf{v} \cdot \mathbf{a} + \mathbf{a} \cdot (\nabla\mathbf{v})^T - 2(\mathbf{A} : \nabla\mathbf{v})$.

4.1 LVE fractional model

Since the extra-stress tensor of the suspension is given by

$$\boldsymbol{\tau} = 2\eta\mathbf{D} + 2\eta N_p \left(\mathbf{D} : \mathbf{A}\right) + \beta D_r \left(\mathbf{a} - \frac{\mathbf{I}}{d}\right), \tag{30}$$

and using again the linear closure and the same rationale as in Section 3, we obtain for the general 3D case

$$\boldsymbol{\tau}_{12} \approx \eta\dot{\gamma} + \frac{2}{15}\eta N_p \dot{\gamma} + \beta D_r \mathbf{a}_{12}. \tag{31}$$

On the other hand, the orientation evolution equation reads

$$\dot{\mathbf{a}} = \nabla\mathbf{v}\cdot\mathbf{a} + \mathbf{a}\cdot(\nabla\mathbf{v})^T - 2\mathbf{A} : \mathbf{D} - 6D_r \frac{d^{1-\alpha}}{dt^{1-\alpha}} \left(\mathbf{a} - \frac{\mathbf{I}}{d}\right). \tag{32}$$

With the notations $\mathbf{a}_{12} \equiv a$ and $\boldsymbol{\tau}_{12} \equiv \tau$, the LVE fractional model thus yields

$$\begin{cases} \tau \approx \eta\dot{\gamma} + \frac{2}{15}\eta N_p \dot{\gamma} + \beta D_r a \\ \frac{da}{dt} \approx \frac{\dot{\gamma}}{5} - 6D_r \frac{d^{1-\alpha} a}{dt^{1-\alpha}} \end{cases}. \tag{33}$$

As in Section 3.1, we apply the small amplitude oscillation $\gamma(t) = \gamma_0 e^{i\omega t}$. From the second equation in (33), we expect that $a(t)$ has the same oscillation frequency but with a certain phase delay φ, that is

$$a = a_0 e^{i\omega t - i\varphi} = \tilde{a}_0 e^{i\omega t}. \tag{34}$$

With the notations $\lambda = \frac{1}{6D_r}$ and $\mu = \frac{1}{30D_r}$, we obtain

$$i\omega\lambda\tilde{a}_0 + (i\omega)^{1-\alpha}\tilde{a}_0 = i\omega\mu\gamma_0, \tag{35}$$

where $i^{1-\alpha} = \chi + i\nu$, with $\chi^2 + \nu^2 = 1$. Thus, Eq. (35) can be rewritten as

$$i\omega\lambda\tilde{a}_0 + (\chi + i\nu)\omega^{1-\alpha}\tilde{a}_0 = i\omega\mu\gamma_0, \tag{36}$$

from which we have

$$\begin{aligned} \tilde{a}_0 =& \gamma_0 \left(\frac{\lambda\mu\omega^2 + \mu\nu\omega^{2-\alpha}}{\chi^2\omega^{2(1-\alpha)} + (\omega\lambda + \nu\omega^{1-\alpha})^2}\right. \\ &\left. + i\frac{\mu\chi\omega^{2-\alpha}}{\chi^2\omega^{2(1-\alpha)} + (\omega\lambda + \nu\omega^{1-\alpha})^2}\right). \end{aligned} \tag{37}$$

Note that for the case of the integer model $\alpha = 1$, we have $\chi = 1$ and $\nu = 0$, and the previous expression reduces to the one considered in Section 3.

From Eq. (37), we go back to the stress expression (first equation in (33)) and write the complex stress amplitude according to

$$\begin{aligned} \tilde{\tau} = \gamma_0 \Bigg(& i\omega\eta \left(1 + \frac{2}{15}N_p\right) + \\ & \beta D_r \left(\frac{\lambda\mu\omega^2 + \mu\nu\omega^{2-\alpha}}{\chi^2\omega^{2(1-\alpha)} + (\omega\lambda + \nu\omega^{1-\alpha})^2} + \right. \\ & \left. i\frac{\mu\chi\omega^{2-\alpha}}{\chi^2\omega^{2(1-\alpha)} + (\omega\lambda + \nu\omega^{1-\alpha})^2}\right)\Bigg), \end{aligned} \tag{38}$$

from which we identify the storage and loss moduli,

$$G' = \beta D_r \frac{\lambda\mu\omega^2 + \mu\nu\omega^{2-\alpha}}{\chi^2\omega^{2(1-\alpha)} + (\omega\lambda + \nu\omega^{1-\alpha})^2}, \tag{39}$$

and

$$\begin{aligned} G'' =& \omega\eta \left(1 + \frac{2}{15}N_p\right) + \\ & \beta D_r \frac{\mu\chi\omega^{2-\alpha}}{\chi^2\omega^{2(1-\alpha)} + (\omega\lambda + \nu\omega^{1-\alpha})^2}. \end{aligned} \tag{40}$$

At small frequencies, the predicted storage modulus G' scales as ω^α, i.e. with the power α of the applied frequency. Thus, it suffices to select $\alpha = 0.6$ to describe the observed experimental behavior in the framework of a consistent linear and single-mode theory.

4.2 Step strain fractional model

As in Section 3.2, the stress relaxation after a step strain is given by

$$\tau = \beta D_r a, \tag{41}$$

where the evolution of a is now calculated from

$$\frac{da}{dt} = -6D_r \frac{da^{1-\alpha}}{dt^{1-\alpha}}, \tag{42}$$

instead of using the standard integer model (22). The numerical solution of Eq. (42) injected into Eq. (41) yields a prediction of stress relaxation.

As shown in the next section, use of the fractional model indeed leads to a power-law behaviour in agreement with the experimental findings.

5 Fractional model predictions versus experimental data

In what follows, we discuss predictions of the proposed fractional model in terms of the LVE storage modulus G' and the step strain modulus G.

The fractional model has 3 parameters: (i) the derivative order α, (ii) the diffusion coefficient D_r, and (iii) the parameter β that quantifies the stress response.

The derivative order α can be identified easily as it determines the slopes of G' and G. Coefficient D_r and β are adjusted for fitting the experimental data.

Figures 3 and 4 depict the global behaviour of the storage modulus for different values of derivative order α and coefficient D_r, respectively. Figures 5 and 6 depict similar predictions for the time evolution of G in step strain.

Finally, the fractional model fitting of LVE and step strain experimental data was performed by considering $\alpha = 0.6$, $D_r = 15$ and $\beta = 190$. Figures 7 and 8 depict the fit for, respectively, the storage modulus and the step strain relaxation. An excellent agreement is obtained, giving us confidence as to the relevance of the proposed fractional model.

6 Conclusions

We have revisited in this paper the rheological modeling of chemically treated CNT suspensions, first addressed in Ma et al. (2009). It was noticed in LVE experiments that such suspensions exhibit mild elasticity characterized by a storage modulus scaling with the power 0.6 of the applied frequency.

The elasticity resulting from standard Brownian rotary diffusion is unable to match these experimental

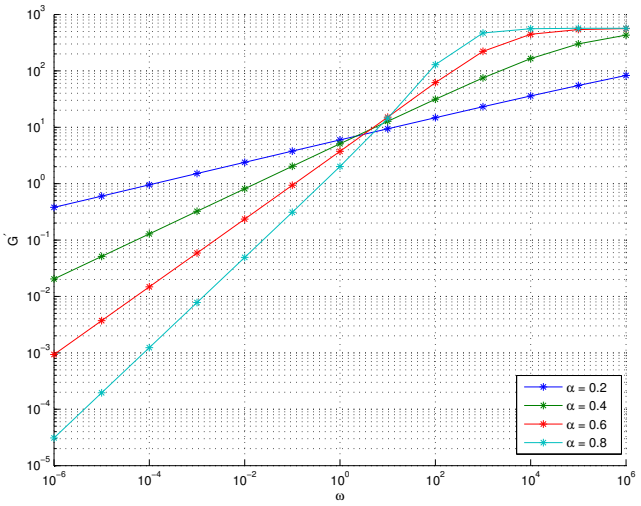

Fig. 3 LVE storage modulus for different values of the derivative order ($D_r = 15$ and $\beta = 190$)

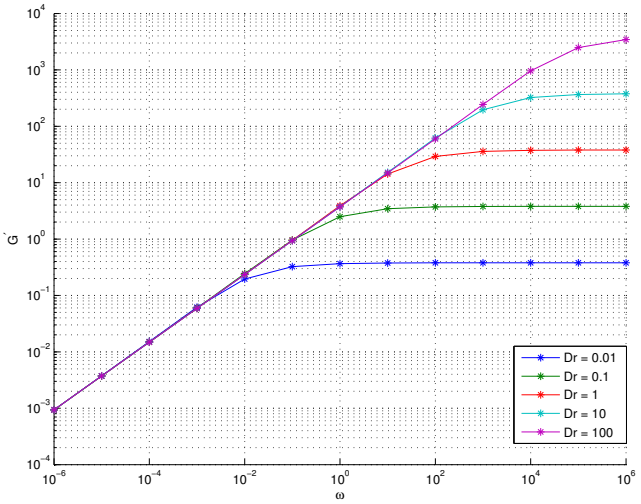

Fig. 4 LVE storage modulus for different values of coefficient D_r ($\alpha = 0.6$ and $\beta = 190$)

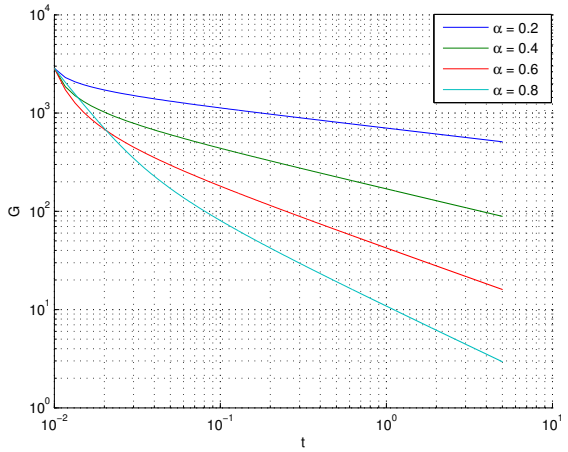

Fig. 5 Step strain modulus for different values of the derivative order ($D_r = 15$ and $\beta = 190$)

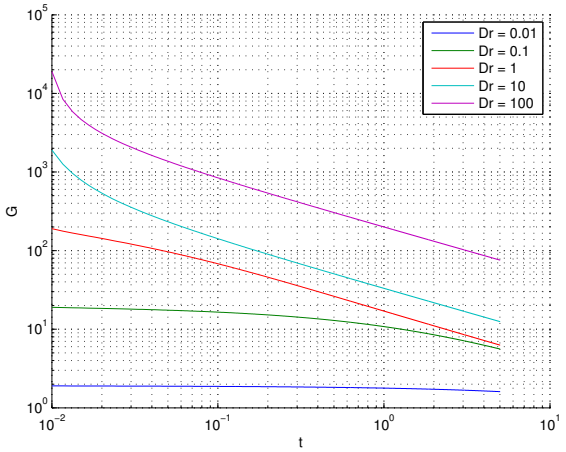

Fig. 6 Step strain modulus for different values of coefficient D_r ($\alpha = 0.6$ and $\beta = 190$)

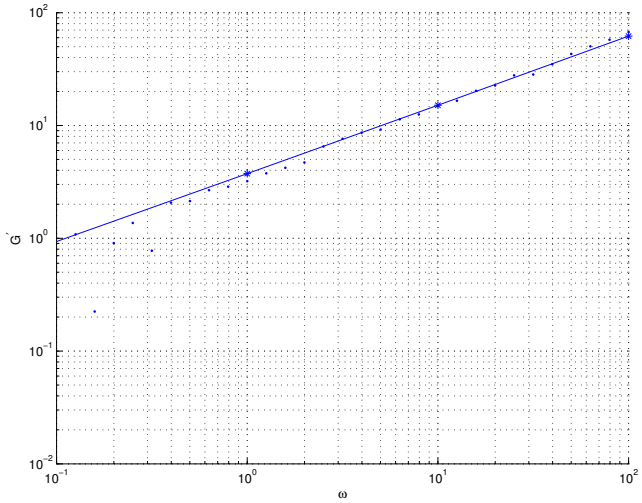

Fig. 7 LVE storage modulus: prediction of fractional model ($\alpha = 0.6$, $D_r = 15$ and $\beta = 190$) versus experimental data

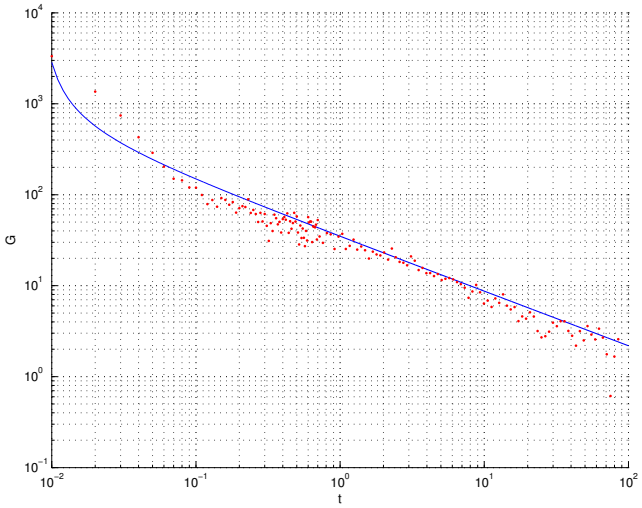

Fig. 8 Step strain modulus: prediction of fractional model ($\alpha = 0.6$, $D_r = 15$ and $\beta = 190$) versus experimental data

data by considering a single-mode model. Obviously one possibility consists in introducing a spectrum of relaxation times able to fit available data, but such an approach is difficult to support physically.

Many authors noticed the existence of anomalous diffusion mechanisms and proposed to model these phenomena by means of models involving fractional (non-integer) derivatives. In this work, we followed a similar route for modeling LVE and step strain behaviour of chemically treated CNT suspensions. We have shown that a single-mode fractional derivative description of rotary diffusion with a derivative order $\alpha = 0.6$ suffices for describing the available experimental data.

A On fractional derivatives

There are many books on fractional calculus and fractional differential equations (e.g. Kilbas et al. (2006) Podlubny (1999)). We summarize here the main concepts needed to understand the developments carried out in this paper.

We start with the formula usually attributed to Cauchy for evaluating the n-th integration, $n \in \mathbb{N}$, of a function $f(t)$:

$$J^n f(t) := \int \cdots \int_0^t f(\tau)\, d\tau = \frac{1}{(n-1)!} \int_0^t (t-\tau)^{n-1} f(\tau)\, d\tau. \tag{43}$$

This can be rewritten as

$$J^n f(t) = \frac{1}{\Gamma(n)} \int_0^t (t-\tau)^{n-1} f(\tau)\, d\tau, \tag{44}$$

where $\Gamma(n) = (n-1)!$ is the gamma function. The latter being in fact defined for any real value $\alpha \in \mathbb{R}$, we can define the fractional integral from

$$J^\alpha f(t) := \frac{1}{\Gamma(\alpha)} \int_0^t (t-\tau)^{\alpha-1} f(\tau)\, d\tau. \tag{45}$$

Now, if we consider the fractional derivative of order α, we select an integer $m \in \mathbb{N}$ such that $m-1 < \alpha < m$, and it suffices to consider an integer m-order derivative combined with a $(m-\alpha)$ fractional integral. Obviously, we could take the derivative of the integral or the integral of the derivative, resulting in the left and right-hand definitions of the fractional derivative usually denoted by $D^\alpha f(t)$ and $D^\alpha_* f(t)$ respectively.

Because these approaches to the fractional derivative began with an expression for the repeated integration of a function, one could consider a similar approach for the derivative. This was the route considered by Grunwald and Letnikov – GL – that defined the so-called 'differintegral' that leads to the fractional counterpart of the usual finite differences. In the present work we use the GL definition of the fractional derivative.

It turns out that the composition of fractional derivatives follows a rule similar to that that for standard derivatives. On the other hand, the Fourier transform of a fractional derivative of order α reads $\mathcal{F}(g(t);\omega) = (i\omega)^\alpha \mathcal{G}(\omega)$. This property is particularly useful when addressing harmonic responses as in the case of LVE experiments.

B Derivation of the fractional derivative of the orientation tensor

We discuss the contribution of fractional diffusion to the rod rotary velocity (the flow induced contribution remains unchanged):

$$\left.\frac{d^\alpha \mathbf{p}}{dt^\alpha}\right|^B = -D_r \frac{\frac{\partial \psi}{\partial \mathbf{p}}}{\psi}. \tag{46}$$

Now, we consider the second-order orientation tensor

$$\mathbf{a} = \int_{\mathcal{S}} \mathbf{p} \otimes \mathbf{p}\ \psi\ d\mathbf{p} \tag{47}$$

whose time derivative can be rewritten as

$$\dot{\mathbf{a}}|^B = \frac{d^{1-\alpha}}{d^{1-\alpha}} \left\{ \frac{d^\alpha}{dt^\alpha} \left\{ \int_{\mathcal{S}} (\mathbf{p}\otimes\mathbf{p} + \mathbf{p}\otimes\mathbf{p})\, \psi\ d\mathbf{p} \right\} \right\}, \tag{48}$$

or

$$\dot{\mathbf{a}}|^B = \frac{d^{1-\alpha}}{d^{1-\alpha}} \left\{ \int_{\mathcal{S}} \frac{d^\alpha}{dt^\alpha} (\mathbf{p}\otimes\mathbf{p} + \mathbf{p}\otimes\mathbf{p})\, \psi\ d\mathbf{p} \right\}. \tag{49}$$

Considering the first term of the Leibnitz's rule related to the fractional derivative of a product of functions (it is easy to prove that the second one leads to the standard diffusion integer term while the others can be neglected), we obtain

$$\dot{\mathbf{a}}|^B \approx \frac{d^{1-\alpha}}{d^{1-\alpha}} \left\{ \int_{\mathcal{S}} \left(\frac{d^\alpha \mathbf{p}}{dt^\alpha} \otimes \mathbf{p} + \mathbf{p} \otimes \frac{d^\alpha \mathbf{p}}{dt^\alpha} \right) \psi\ d\mathbf{p} \right\}, \tag{50}$$

or

$$\dot{\mathbf{a}}|^B \approx -D_r \frac{d^{1-\alpha}}{d^{1-\alpha}} \left\{ \int_{\mathcal{S}} \left(\frac{\frac{\partial \psi}{\partial \mathbf{p}}}{\psi} \otimes \mathbf{p} + \mathbf{p} \otimes \frac{\frac{\partial \psi}{\partial \mathbf{p}}}{\psi} \right) \psi\ d\mathbf{p} \right\}, \tag{51}$$

which finally gives

$$\dot{\mathbf{a}}|^B \approx -2dD_r \frac{d^{1-\alpha}}{d^{1-\alpha}} \left(\mathbf{a} - \frac{\mathbf{I}}{d} \right). \tag{52}$$

References

Abisset-Chavanne, E., Chinesta, F., Ferec, J., Ausias, G., Keunings, R. On the multiscale description of dilute suspensions of non-Brownian rigid clusters composed of rods. Journal of Non-Newtonian Fluid Mechanics, In press, 2014.

Advani, S., Tucker Ch. The use of tensors to describe and predict fiber orientation in short fiber composites. J Rheol., **31**, 751-784, 1987.

Advani, S., Tucker, Ch. Closure approximations for three-dimensional structure tensors, J. Rheol., **34**, 367-386, 1990.

Amari, T., Watanabe, K. Stress relaxation of carbon black-linseed oil suspensions, J. Soc. Rheol. Jpn. **8**, 80-83, 1980.

Carter, L.F. A study of the rheology of suspensions of rod-shaped particles in a Navier-Stokes liquid, Ph.D. dissertation, University of Michigan, Ann Arbor, 1967.

Chinesta, F. From single-scale to two-scales kinetic theory descriptions of rods suspensions. Archives in Computational Methods in Engineering, **20**, 1-29, 2013.

Cueto, E., Ma, A.W.K., Chinesta, F., Mackley, M.R. Numerical simulation of spin coating processes involving functionalised Carbon nanotube suspensions, International Journal of Material Forming, **1**, 89-99, 2008.

Cueto, E., Monge, R., Chinesta, F., Poitou, A., Alfaro, I., Mackley, M.R. Rheological modeling and forming process simulation of CNT nanocomposites, International Journal of Material Forming, **3**, 1327-1338, 2010.

Cruz, C., Illoul, L., Chinesta, F., Regnier, G. Effects of a bent structure on the linear viscoelastic response of Carbon Nanotube diluted suspensions, Rheologica Acta, **49**, 1141-1155, 2010.

Cruz, C., Chinesta, F., Regnier, G. Review on the Brownian dynamics simulation of bead-rod-spring models encountered in computational rheology, Archives of Computational Methods in Engineering, **19/2**, 227-259, 2012.

Dupret, F., Verleye, V. Modelling the flow of fibre suspensions in narrow gaps, in D.A. Siginer, D. De Kee, R.P. Chabra (Ed.), Advances in the Flow and Rheology of Non-Newtonian Fluids, Rheology Series, Elsevier, 1347-1398, 1999.

Ganani, E., Powell, R.L. Rheological properties of rodlike particles in a Newtonian and non-Newtonian fluid, Journal of Rheology **30**, 995-1013, 1986.

Jaishankar, A., McKinley, G.H. Power-law rheology in the bulk and at the interface: quasi-properties and fractional constitutive equations. Proc. R. Soc., 2012.

Jeffery, G.B. The motion of ellipsoidal particles immersed in a viscous fluid, Proc. R. Soc. London, **A102**, 161-179, 1922.

Kilbas, A., Srivastava, H.M., Trujillo, J.J. Theory and applications of fractional differential equations, Elsevier, 2006.

Kroger, M., Ammar, A., Chinesta, F. Consistent closure schemes for statistical models of anisotropic fluids, Journal of Non-Newtonian Fluid Mechanics, **149**, 40-55, 2008.

Ma, A., Chinesta, F., Mackley, M.R., Ammar, A. The rheological modelling of Carbon Nanotube (CNT) suspensions in steady shear flows, International Journal of Material Forming, **2**, 83-88, 2008.

Ma, A., Chinesta, F., Ammar, A., Mackley, M.R. Rheological modelling of Carbon Nanotube aggregate suspensions, Journal of Rheology, **52/6**, 1311-1330, 2008.

Ma, A., Chinesta, F., Mackley, M.R. The rheology and modelling of chemically treated Carbon Nanotube suspensions, Journal of Rheology, **53/3**, 547-573, 2009.

Mewis, J., Meire, C. Yielding in weakly flocculated systems. in Mena, B., Garcia-Rejon, A., Rangel-Nafaille, C. (Ed.) Advances in Rheology, Volume 2: Fluids, Elsevier, 1984.

Podlubny, I. Fractional differential equations, Academic Press, San Diego, 1999.

Rahatekar, S.S., Koziol, K.K., Butler, S.A., Elliott, J.A., Shaffer, M.S.P., Mackley, M.R., Windle, A.H. Optical microstructure and viscosity enhancement for an epoxy resin matrix containing multi-wall Carbon Nanotubes, Journal of Rheology, **50**, 599-610, 2006.

Strautins, U., Latz, A. Flow-driven orientation dynamics of semiflexible fiber systems, Rheol Acta, **46**, 1057-1064, 2007.

Song, Y.K., Youn, J.R. Influence of dispersion states of Carbon Nanotubes on physical properties of epoxy nanocomposites, Carbon, **43**, 1378-1385, 2005.

Xu, J.S., Chatterjee, S., Koelling, K.W., Wang, Y., Bechtel, S.E. Shear and extensional rheology of Carbon Nanofibers suspensions, Rheologica Acta, **44**, 537-562, 2005.

Yearsley, K.M., Mackley, M.R., Chinesta, F., Leygue, A. The rheology of multiwalled carbon nanotube and carbon black suspensions, **56**, 1465-1490, 2012.